Daily rhythms of glycerophospholipid synthesis in fibroblast cultures involve differential enzyme contributions[S]

Victoria A. Acosta-Rodríguez,* Sebastián Márquez,* Gabriela A. Salvador,† Susana J. Pasquaré,† Lucas D. Gorné,* Eduardo Garbarino-Pico,* Norma M. Giusto,† and Mario Eduardo Guido[1,*]

CIQUIBIC-CONICET,* Departamento de Química Biológica, Facultad de Ciencias Químicas, Universidad Nacional de Córdoba, Córdoba, Argentina; and INIBIBB-CONICET,† Universidad Nacional del Sur, Bahía Blanca, Argentina

Abstract **Circadian clocks regulate the temporal organization of several biochemical processes, including lipid metabolism, and their disruption leads to severe metabolic disorders. Immortalized cell lines acting as circadian clocks display daily variations in [^{32}P]phospholipid labeling; however, the regulation of glycerophospholipid (GPL) synthesis by internal clocks remains unknown. Here we found that arrested NIH 3T3 cells synchronized with a 2 h-serum shock exhibited temporal oscillations in *a*) the labeling of total [^{3}H] GPLs, with lowest levels around 28 and 56 h, and *b*) the activity of GPL-synthesizing and GPL-remodeling enzymes, such as phosphatidate phosphohydrolase 1 (PAP-1) and lysophospholipid acyltransferases (LPLAT), respectively, with antiphase profiles. In addition, we investigated the temporal regulation of phosphatidylcholine (PC) biosynthesis. PC is mainly synthesized through the Kennedy pathway with choline kinase (ChoK) and CTP:phosphocholine cytidylyltranferase (CCT) as key regulatory enzymes. We observed that the PC labeling exhibited daily changes, with the lowest levels every ~28 h, that were accompanied by brief increases in CCT activity and the oscillation in ChoK mRNA expression and activity.[JLR] Results demonstrate that the metabolisms of GPLs and particularly of PC in synchronized fibroblasts are subject to a complex temporal control involving concerted changes in the expression and/or activities of specific synthesizing enzymes.**—Acosta-Rodríguez, V. A., S. Márquez, G. A. Salvador, S. J. Pasquaré, L. D. Gorné, E. Garbarino-Pico, N. M. Giusto, and M. E. Guido. **Daily rhythms of glycerophospholipid synthesis in fibroblast cultures involve differential enzyme contributions. *J. Lipid Res.* 2013.** 54: **1798–1811.**

Supplementary key words phospholipid • circadian rhythm • serum shock • synchronization

This work was supported by Agencia Nacional de Promoción Científica y Tecnológica (FONCyT) (PICT 2004 N 967, PICT 2006 N 898, and PICT 2010 N 647); Secretaría de Ciencia y Técnica-Universidad Nacional de Córdoba (SeCyT-UNC); Consejo Nacional de Investigaciones Científicas y Tecnológicas de Argentina (CONICET); Ministerio de Ciencia y Técnica de Córdoba; Fundación Antorchas; y Florencio Fiorini.

Manuscript received 28 November 2013 and in revised form 17 April 2013.

Published, JLR Papers in Press, May 2, 2013
DOI 10.1194/jlr.M034264

Circadian clocks are present in most living organisms and regulate a number of physiological and behavioral rhythms with a period near 24 h (1). In mammals, a master pacemaker located in the hypothalamic suprachiasmatic nuclei (SCN) and a number of peripheral oscillators distributed in different organs and tissues have been described (2). Moreover, several types of isolated single cells, immortalized cell lines, and primary cell cultures present rhythms in gene expression and metabolic activities (3–5) (supplementary Fig. IA). At the molecular level, the clock is controlled by a transcriptional/translational feedback circuitry that generates circadian patterns of gene expression (2). Several transcriptomic, proteomic, and metabolomic studies in different mammalian tissues and cultured cells reveal a strong crosslink between the metabolism and the circadian clock (6–13). In fact, circadian clocks located throughout the body govern a wide array of physiological

Abbreviations: CCT, CTP:phosphocholine cytidylyltranferase; CDP-Cho, cytidine diphosphate choline; CDP-DAG, cytidinediphosphate-DAG; CDP-Etn, cytidine diphosphate ethanolamine; CDS, CDP-diacylglycerol synthase; Cho, choline; ChoK, choline kinase; CL, cardiolipin; CLS, cardiolipin synthase; CPT, CDP-choline:diacylglycerol cholinephosphotransferase; DAG, diacylglycerol; DAGK, diacylglycerol kinase; EK, ethanolamine kinase; EPT, CDP-ethanolamine:diacylglycerol ethanolaminephosphotransferase; ET, CTP:phosphoethanolamine cytidylyltransferase; Etn, ethanolamine; G3P, glycerol 3-phosphate; GPAT, acyl-CoA:glycerol-3-phosphate acyltransferase; GPL, glycerophospholipid; LCL, lysocardiolipin; LPA, lysophosphatidic acid; LPC, lysophosphatidylcholine; LPE, lysophosphatidylethanolamine; LPG, lysophosphatidylglycerol; LPI, lysophosphatidylinositol; LPAAT, lysophosphatidic acid acyltransferase; LPLAT, lysophospholipid acyltransferase; LPS, lysophosphatidylserine; MAG, monoacylglycerol; P-Cho, phosphocholine; PA, phosphatidic acid; PAP, phosphatidate phosphohydrolase; PC, phosphatidylcholine; PE, phosphatidylethanolamine, PEMT, phosphatidylethanolamine methyl transferase; PG, phosphatidylglycerol; PGP, phosphatidylglycerol phosphate; PGPP, PGP phosphatase; PGPS, PGP synthase; PI, phosphatidylinositol; PIS, PI synthase; PLA, phospholipase A; PS, phosphatidylserine; PSD, phosphatidylserine decarboxylase; PSS1, phosphatidylserine synthase 1.

[1]To whom correspondence should be addressed.
e-mail: mguido@fcq.unc.edu.ar

[S] The online version of this article (available at http://www.jlr.org) contains supplementary data in the form of three figures.

functions, including those related to lipid metabolism (9–11, 14). Disruption of circadian clocks at the molecular level leads to metabolic disorders, including obesity and diabetes (15–20).

Glycerophospholipids (GPL) are essential structural components of all biological membranes and bioactive molecules involved in cellular functions, such as cell signaling, energy balance, vesicular transport, and cell-to-cell communication (21, 22). GPLs are first synthesized from glycerol-3-phosphate via de novo pathway described by Kennedy and Weiss in 1956 (22, 23) (see Scheme 1) and then undergo maturation in the remodeling pathway (Lands cycle) as a result of the concerted action of phospholipase A (PLA) and lysophospholipid acyl transferases (LPLAT) (24, 25).

As a fundamental phospholipid in all eukaryotic membranes, phosphatidylcholine (PC) plays an important role in the structural composition of membranes and in the generation of second messengers involved in key regulatory functions and other processes (26–28). PC synthesis is crucial for cell growth, proliferation, and survival (29). In mammals, the disruption of genes encoding phospholipid biosynthetic enzymes has severe physiological consequences or lethality (30). In most nucleated cells, the biosynthesis of PC occurs via the Kennedy pathway, involving three enzymatic steps catalyzed by choline kinase (ChoK), CTP:phosphocholine cytidylyltranferase (CCT), and CDP-choline:1,2-diacylglycerol cholinephosphotransferase (CPT) (Scheme 1). CCT activity is considered to be the rate-limiting and regulatory step under most metabolic conditions (31). However, it has been demonstrated that the availability of diacylglycerol (DAG) and regulation of ChoK also influence PC biosynthesis (27, 32, 33). In most mammals, there are two genes encoding for ChoK: *Chka* codes for ChoKα1/2 and *Chkb* codes for ChoKβ (34, 35). Mice lacking *ChoKα* die early in embryogenesis, whereas mice lacking *ChoKβ* survive to adulthood (30). ChoK overexpression has been implicated in the development of human carcinogenic processes (36, 37). In mice, there are two genes for CCT: *Pcyt1a* encodes the CCTα protein from alternative transcripts termed CCTα1 and CCTα2, and the *Pcyt1b* gene encodes the CCTβ2 and CCTβ3 proteins from the differentially alternative spliced mRNAs CCTβ2 and CCTβ3 (38).

Several studies have reported the regulation of PC biosynthesis during the cell cycle, which is consistent with a higher PC mass requirement prior to mitosis (39). In addition, one report showed day/night changes in the content of PC and other phospholipids in the cerebral cortex of rats maintained under a light-dark cycle (40). Nevertheless, the synthesis of PC has not yet been investigated under constant environmental conditions to reveal whether temporal changes may be generated in an endogenous and self-sustained manner as expected for circadian rhythms. In this regard, we have previously demonstrated that de novo synthesis of whole phospholipids in retinal neurons in vivo or in vitro (41–43) and in quiescent fibroblasts synchronized by a serum shock is controlled by a circadian clock (4, 14).

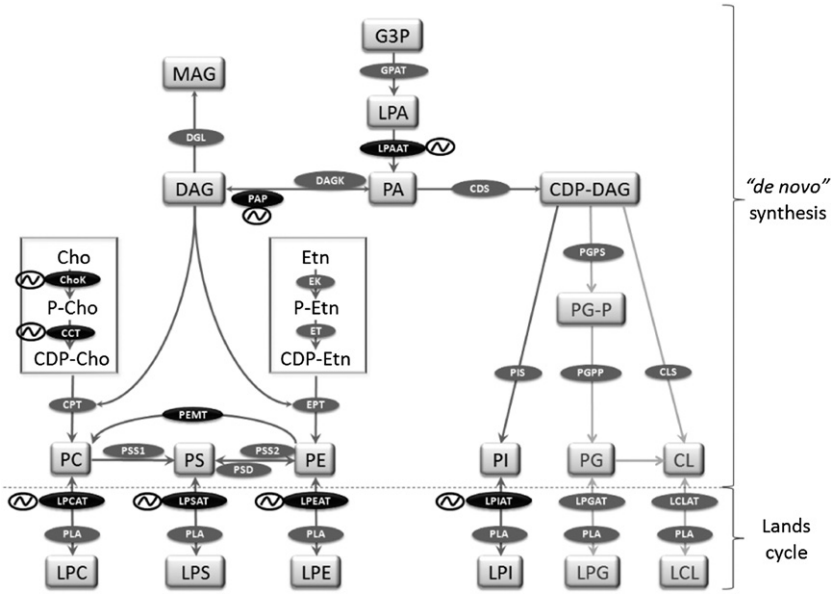

Scheme 1. Pathways of GPL biosynthesis in eukaryotic cells: temporal regulation of GPL-synthesizing enzyme activities. GPLs are first synthesized through the de novo pathway (Kennedy pathway) and then modified through the remodeling pathway (Lands cycle). The steps labeled with the tilde (~) indicate a significant temporal variation. Names within rectangles correspond to intermediate substrates and reaction products for GPL synthesis, and names within dark ovals denote enzymes exhibiting a daily variation. See text for details. Reaction substrates and products: CDP-Cho, CDP-DAG, CDP-Etn, Cho, CL, DAG, Etn, G3P, LCL, LPA, LPC, LPE, LPG, LPI, LPS, MAG, P-Cho, PA, PC, PE, PG, PGP, PI, and PS. Enzymes: CCT, CDS, CPT, CLS, EK, EPT, ET, GPAT, LPAAT, PAP, PEMT, PGPS, PGPP, PIS, and PLA.

In this work, we investigated whether the GPL metabolism is temporally regulated at early steps of de novo biosynthesis and remodeling. In addition, we addressed whether the synthesis of PC changes throughout the day and, if so, how this event may be regulated. To this end, we performed circadian studies in arrested NIH 3T3 cells after serum shock synchronization. We first examined the temporal regulation of total GPLs by metabolic labeling with [^{3}H]glycerol as a precursor and the activity of phosphatidate phosphohydrolase 1 (PAP-1) in desphosphorylating phosphatidic acid (PA) to DAG, a branching point for de novo synthesis of all GPLs. We then assayed LPLAT activities involved in the remodeling of membrane phospholipids. Finally, we evaluated possible changes across time in PC biosynthesis by metabolic labeling with [^{32}P] phosphate and [^{3}H]glycerol, as well as the activity and expression of the two key synthesizing enzymes, ChoK and CCT.

EXPERIMENTAL PROCEDURES

Materials

All reagents were analytical grade. [^{32}P]Na_2 orthophosphate (specific activity 285.5 Ci/mg), [methyl-^{14}C]phosphorylcholine (specific activity 55 mCi/mmol), [methyl-^{14}C]choline chloride (specific activity 55.19 mCi/mmol 0.2 mCi/ml), and [2-^{3}H]glycerol were purchased from NEN Life Science Products (Boston, MA). Alugram SIL G/UV_{254} TLC silica gel 60 precoated sheets were from Macherey-Nagel (Duren, Germany). Phospholipid standards, $MgCl_2$, and ATP were from Sigma (St. Louis, MO). The antibody against α-tubulin was the monoclonal DM1A purchased from Sigma (dilution 1:1,000). Polyclonal antibodies anti-CCTα and anti-CCTβ2 (epitope B2 that recognizes N-terminal of CCTβ2, dilution 1:200) used for ICC were a generous gift from Dr. Susan Jackowski (St. Jude Children's Research Hospital, Memphis, TN). Secondary antibodies used for immunocytochemistry (ICC, dilution 1:1000) were anti-mouse Alexa Fluor 488, anti-rabbit Alexa Fluor 546, and ProLong antifade kit with mounting medium from Molecular Probes (Eugene, OR). Primary antibodies used for Western blot were Prestige Antibody Anti-PCYT1B (Sigma HPA006367) for CCTβ2/3 isoform (dilution 1:200) and polyclonal rabbit anti-CCTα generously donated by Dr. N. Ridgway [Dalhousie University, Halifax, NS, Canada; dilution 1:3000 (44)]. The secondary antibodies used for Western blot were anti-rabbit IgG IRDye®800CW conjugated goat polyclonal and anti-mouse IgG IRDye®680CW conjugated goat polyclonal from Li-COR® IRDye® Infra-Red Imaging Reagents (dilution 1:25,000). Bio-Rad protein assay based on the Bradford method was used to measure the protein concentration (45).

Cell cultures

NIH 3T3 fibroblasts were grown in DMEM (Gibco) supplemented with 10% calf serum (Gibco). Cells reached confluence after ~4 days in a CO_2 incubator at 37°C. At time 0, the medium was changed to 50% horse serum (Gibco-BRL)-rich medium. After 2 h, the medium was replaced with serum-free DMEM or DMEM plus 0.5% calf serum and maintained under this condition for several days according to Balsalobre et al. (3, 4).

Phospholipid labeling

The incorporation of [^{32}P]orthophosphate or [^{3}H]glycerol into phospholipids of NIH 3T3 fibroblasts in culture was assessed at different times across several cycles of 28 h, each ranging from 0.5 to 60 h. A 30 min labeling pulse of [^{32}P]Na_2Orthophosphate (10 μCi/well) or [^{3}H]glycerol (8.5 μCi/well) was given to cultures at different times after the serum shock. Cells were harvested 30 min after addition of the radioactive precursor to the cultures at the different phases assessed and processed for phospholipid labeling.

Determination of radioactivity in phospholipids

The labeling of phospholipids was determined according to Guido and Caputto by the TCA-PTA method (46). Total phospholipids were extracted with chloroform/methanol (2:1, v/v), and radioactivity was determined in a liquid scintillation counter.

Chromatographic separation of individual phospholipids

Individual phospholipids were separated in silica gel 60 plates (Macherey-Nagel; Duren, Germany) by a one-dimensional, two-solvent system procedure described in Weiss et al. (47). Standards and individual lipid species were visualized with iodine vapors. Radioactivity incorporated into individual lipids was assessed by autoradiography. The band corresponding to PC at different phases was scraped from the silica plate, and [^{3}H]radioactivity was determined in vials with 2 ml of scintillation liquid in a scintillation counter.

In vitro determination of LPLAT

Confluent NIH 3T3 fibroblasts from 100 mm dishes were collected at different times from 7 to 56 h after serum shock in PBS, lyophilized, and resuspended in H_2O containing protease inhibitors. Cell lysates were used as a source of enzyme and endogenous lysophospholipids for determination of total LPLAT activity. The activity of NIH 3T3 fibroblast LPLAT was determined as an "in vitro" labeling by measuring the incorporation of [^{14}C]oleate from [^{14}C]oleoyl-CoA (56 mCi/mmol) into different endogenous lysophospholipid acceptors as described in Castagnet and Giusto (48) and Garbarino-Pico et al. (42). Under these experimental conditions, changes in the activity assessed may reflect both changes in the amount of active enzyme and in the content of endogenous lysophospholipids. The incubation mixture for the assay contained 60 mM Tris-HCl (pH 7.8), 4 μM [1-^{14}C]oleoyl-CoA (10^5 dpm/assay), 10 mM $MgCl_2$, 10 mM ATP, 75 μM CoA, and 80 μg of cellular homogenates in a final volume of 150 μl. The reaction was incubated for 10 min with shaking at 37°C and stopped by addition of 5 ml chloroform/methanol (2:1, v/v). The lipids were extracted according to the method of Folch et al. (49). The lipid extract was dried under N_2, resuspended in chloroform/methanol (2:1, v/v), and spotted on silica gel H plates. Unlabeled phospholipids were used as standards. The chromatograms were developed by two-dimensional TLC using as system solvents chloroform/methanol/ammonia (65:25:5, v/v/v) first and chloroform/acetone/methanol/acetic acid/water (30:40:10:10:4, v/v/v/v/v) for the second dimension, and visualized with iodine vapors. The spots corresponding to PA, PC, phosphatidylethanolamine (PE), phosphatidylinositol (PI), and phosphatidylserine (PS) were scraped off, and radioactivity was determined by liquid scintillation.

Determination of PAP-1 activity

Confluent NIH 3T3 fibroblasts from 100 mm dishes were collected at different times from 7 to 56 h after serum shock in PBS and resuspended in H_2O containing protease inhibitors. PAP-1 activity was determined by monitoring the rate of release of 1,2 diacyl-[2-^{3}H]glycerol (DAG) from [2-^{3}H]phosphatidic acid (PA) as previously described by Pasquaré and Giusto (42, 50, 51). The

reaction was stopped at 20 min by addition of chlorophorm/methanol (2:1, v/v). DAG was separated by TLC and developed with hexane:diethyl ether:acetic acid (35:65:1, v/v/v) (52). To separate monoacylglycerol (MAG) from PA, the chromatogram was developed with hexane/diethyl ether/acetic acid (20:80:2.3, v/v/v) as developing solvent. PAP activity was expressed as the sum of labeled DAG plus MAG (h × mg of protein)$^{-1}$.

In vitro assessment of ChoK enzyme activity

Confluent NIH 3T3 fibroblasts from 100 mm dishes were collected at different times from 7 to 56 h after serum shock in PBS and resuspended in H_2O plus protease inhibitor. Protein homogenate (100 μg) was assessed with 0.5 μl [methyl-^{14}C]choline chloride (55.19 mCi/mmol specific activity), 10 mM ATP, 10 mM Mg^{2+}, 0.1M Tris-HCl (pH 8) according to Weinhold et al. (53). The reaction was stopped at 10 min by addition of 1 ml of chloroform on ice. The soluble products were extracted using chloroform/methanol (2:1, v/v) and separated by TLC. The solvent system was 0.9% NaCl/methanol/NH_4OH (50:70:5, v/v/v). The TLC-separated product was autoradiographed, and the bands corresponding to [^{14}C]choline and [^{14}C]phosphocholine were scraped and quantified by adding 1 ml of scintillation cocktail in a liquid scintillation counter. The time reaction (10 min) and protein concentration (100 μg) were selected from a linear range of time and enzyme curves.

In vitro assessment of CCT enzyme activity

Confluent NIH 3T3 fibroblasts from 100 mm dishes were collected at different times from 0.5 to 36 h after serum shock in sterile water and were sonicated three times for 30 s at 4°C. Cell lysates (100 μg of protein) were used as a source of enzyme for determination of total CCT activity. CCT activity was measured by conversion of phosphoryl [methyl-^{14}C] choline (55.0 mCi/ mmol specific activity) into CDP-[^{14}C] choline according to Vance et al. (54). The reaction was incubated 60 min at 37°C and was stopped by immersion in boiling water for 2 min. The TLC plates were developed in a solvent system composed of CH_3OH:0.6% NaCl:NH_4OH (50:50:5 v/v/v). The CDP-choline was visualized under UV light, scraped, and quantified in a liquid scintillation counter.

RNA isolation and reverse transcription

Total RNA was extracted from NIH 3T3 cells using TRIzol® reagent following the manufacturer´s specifications (Invitrogen). The yield and purity of RNA were estimated by optical density at 260/280 nm. Total RNA (1 μg) was treated with DNase (Promega) and utilized as a template for the cDNA synthesis reaction using ImPromII reverse transcriptase (Promega) and an equimolar mix of random hexamers and oligo-dT (Biodynamics) in a final volume of 25 μl according to the manufacturer´s indications.

PCR assay (endpoint PCR)

The primers used for RT-PCR are listed in **Table 1**. The polymerase chain reaction was performed in a Labnet Multigen Thermal cycler using the GoTaq® DNA Polymerase (Promega). PCR reactions were carried out with an initial denaturation step of 5 min at 94°C, 35 cycles of 30–40 s at 94°C, 30 s at 60°C, 40 s at 72°C, and a final 5 min elongation step at 72°C. Amplification products were separated by 1% agarose gel electrophoresis and visualized by ethidium-bromide staining.

Real-time PCR

Quantitative RT-PCR (qPCR) was performed using SYBR Green or TaqMan Gene Expression assay in a Rotor Q Gene (Qiagen). The primer/probe sequences are summarized in Tables 1 and **2**. The amplification mix contained 1 μl of the cDNA, 1 μl 20× mix primer/probe or 250 nM Forward-Reverse TBP primers, and 10 μL of Master Mix 2× (Applied Biosystem) in a total volume of 20 μL. The cycling conditions were 10 min at 95.0°C, and 40 cycles of 95.0°C for 15 s, 60.0°C for 30 and 72°C for 30 s. The standard curve linearity and PCR efficiency (E) were optimized. We used the Pfaffl quantification method (Real-Time PCR Applications Guide, Bio-Rad), setting samples from cells harvested 35 h after serum shock as calibrator and 18S or TBP as the reference gene.

$$R = \frac{E_{\text{target}}^{C_T(calibrator)-C_T(sample)}}{E_{reference}^{C_T(calibrator)-C_T(sample)}}$$

Each RT-PCR quantification experiment was performed in duplicate (TaqMan) and triplicate (SYBR) for three or four independent experiments.

Immunocytochemistry

The NIH 3T3 were cultured as described previously on 10 mm coverslips to ∼70–80% confluence. At different times after the serum shock, cells were washed twice with cold PBS and fixed in 3% paraformaldehyde/4% sucrose in PBS for 15 min at 37°C. Cells were permeabilized in PBS-0.2% Triton × 100 for 5 min at 37°C, blocked for 2 h with 1% BSA-PBS, and then incubated overnight at 4°C with primary antibodies anti-CCTα, anti-CCTβ2, and anti-α-tubulin in 1% BSA-PBS. Cells were then washed with PBS and incubated with the corresponding secondary antibody Alexa Fluor 488 or Alexa Fluor 546 (1:1000) for 2 h at room temperature, washed, and mounted with Prolong Antiface kit. The slices were visualized by Axioplan fluorescence microscopy (Zeiss, Oberkochen, Germany) equipped with a micromax camera (Princeton Instruments, Trenton, NJ). Relative levels of immunofluorescence associated with CCTα, CCTβ2, and α-tubulin proteins were assessed according to grayscale intensity by using image analysis software Metamorph 6.0 (Universal Imaging Corporation, Downingtown, PA).

Western blot

NIH 3T3 fibroblasts were harvested at different times after the serum shock in radio-immunoprecipitation assay (RIPA) buffer containing protease inhibitor (Sigma). Total protein content in the homogenates was determined by the Bradford method (45). Homogenates were resuspended in sample buffer and heated at 90°C for 5 min. 50 μg of protein were separated by SDS-gel electrophoresis on 12% polyacrylamide gels according to (55). Primary antibodies were incubated overnight at 4°C and secondary antibodies were incubated 1 h at room temperature. Finally the membranes were scanned using an Odyssey IR Imager (LI-COR Biosciences). Densitometric quantification of specific bands was carried out with ImageJ software (National Institute of Health Bethesda, Maryland).

Propidium-iodide staining and flow cytometry

Cells grown to confluence were collected at different times after synchronization (0, 2, and 24 h), washed in cold PBS, and fixed with ice-cold 70% ethanol for at least 24 h. Cell pellets were resuspended in 150 μl of staining solution (PBS containing 50 μg/ml propidium iodide and 10 μg RNase A). Cell-cycle analysis was performed with 60,000 cells on a flow cytometer (DB Bioscience). The analysis program used was ModFit software (Verity Software House, Topsham, ME).

TABLE 1. PCR primer sequences

Transcript Name	Accession Number	Forward Primer (5′ → 3′) Reverse Primer (5′ → 3′)	Amplicon Size (bp)
Tbp	NM_013684.3	AGAACAATCCAGACTAGCGCA [a] GGGAACTTCACATCACAGCTC	100
Bmal1	NM_007489.3	GCAGTGCCACTGACTACCAAGA [b] TCCTGGACATTGCATTGCAT	201
CCTα1	NM_009981	ATTTGACTTCGCTAGTCGGTGAC [c] TCCATCCGCATAAACTCTCACAG	331
CCTα2	AK076830	ACCATGACCGAGTAAGTATGCAGCA [c] TCCATCCGCATAAACTCTCACAG	414
CCTβ2	NM_211138	TGCCTGGGAGGAGACTCCCAGAGGG [c] GGCGCGTCTCTGATGACTTCATCCA	503
CCTβ3	NM_177546	CAGAAATGCAGCATGGACAAGGACG [c] GGCGCGTCTCTGATGACTTCATCCA	371

[a] Extracted from Ref. 76.
[b] Extracted from Ref. 77.
[c] All CCT primer sequences are extracted from Ref. 38.

Statistics

Statistical analyses involved a one-way Kruskal-Wallis ANOVA by ranks to test the time effect. Pairwise comparisons were performed by the Mann-Whitney test when appropriate. For further periodic analysis, we performed a linear-circular correlation with the Spearman coefficient followed by an aleatorization test with 1,000 iterations to determine the *P*-value as described by Mardia et al. (56). The analysis considered a period (τ) of 14, 28, and 35 h and significance at $P < 0.05$.

RESULTS

Characterization of cell culture conditions

To investigate the circadian regulation of GPL synthesis in NIH 3T3 cells, we first characterized the experimental culture conditions. To this end, cells grown to confluence and synchronized with a 2 h serum shock were maintained in a basal serum (≤0.5%) medium for several days.

A synchronization protocol is essential to adjust single cell-autonomous oscillators to the same phase within the culture. Cells synchronized with a brief serum shock displayed a marked circadian rhythmicity in mRNA levels of the clock gene *Bmal1* during 56 h after synchronization (supplementary Fig. IA) as previously reported (3–5). We examined whether cells undergo an important rate of cell division after the serum shock since it may serve as a mitotic stimulus. We found by flow cytometry that most cells were arrested at the G_0/G_1 phases (∼90%), while <1% and ∼9% of cells reached the G_2/M and S phases, respectively (supplementary Fig. IB). The distribution of cell populations throughout the cell cycle remained constant at all times examined (0, 2 and 24 h after stimulation). Remarkably, these two major features - the nonproliferative condition and serum synchronization - make NIH 3T3 cell cultures a very useful model of peripheral oscillator for circadian studies regardless of both cell division and systemic influences from the brain master clock.

Circadian changes in the synthesis of GPLs in synchronized NIH 3T3 fibroblasts

To determine whether the de novo biosynthesis of total phospholipids varies throughout the day, we examined the time course incorporation of [^{3}H]glycerol into GPLs in quiescent NIH 3T3 cells after serum shock. The results showed a significant daily variation in the synthesis of total GPLs ($P < 0.0004$ by ANOVA) (**Fig. 1A** and **Tables 3** and **4**). During the first cycle, we found elevated levels of [^{3}H] GPLs at 4–22 h after serum shock and minimum levels at 29–30 h. The levels increased again at 32 h after synchronization and remained elevated until 48 h, decreasing to minimum values around 54 h (Fig. 1A).

Daily variation in the activity of different NIH 3T3 phospholipid synthesizing enzymes

We explored the possibility that the circadian changes observed in the metabolic labeling of total GPLs in synchronized NIH 3T3 cells were due to variations in the activity of enzymes involved in the de novo synthesis of phospholipids (see Scheme 1). For this, we determined the in vitro activities of lysophosphatidic acid acyltranferase (LPAAT) and PAP-1 in homogenates of synchronized NIH

TABLE 2. Gene expression assays

Transcript Name	Accession Number	TaqMan Gene Expression Assay (Applied Biosystems)	Amplicon Size (bp)
ChoKα	NM_013490.3	Mm00442760_m1	73
ChoKβ	NM_007692.6	Mm00432498_m1	72
CCTα	NM_009981.4	Mm00447772_m1	96
CCTα/β	NM_211138.1	Mm01236989_m1	87
Pemt	NM_008819.2	Mm00839436_m1	82
Lipin-1	NM_001130412.1 NM_172950.3 NM_015763.4	Mm00522212_m1	93
18S rRNA	X03205.1	Hs99999901_s1	187

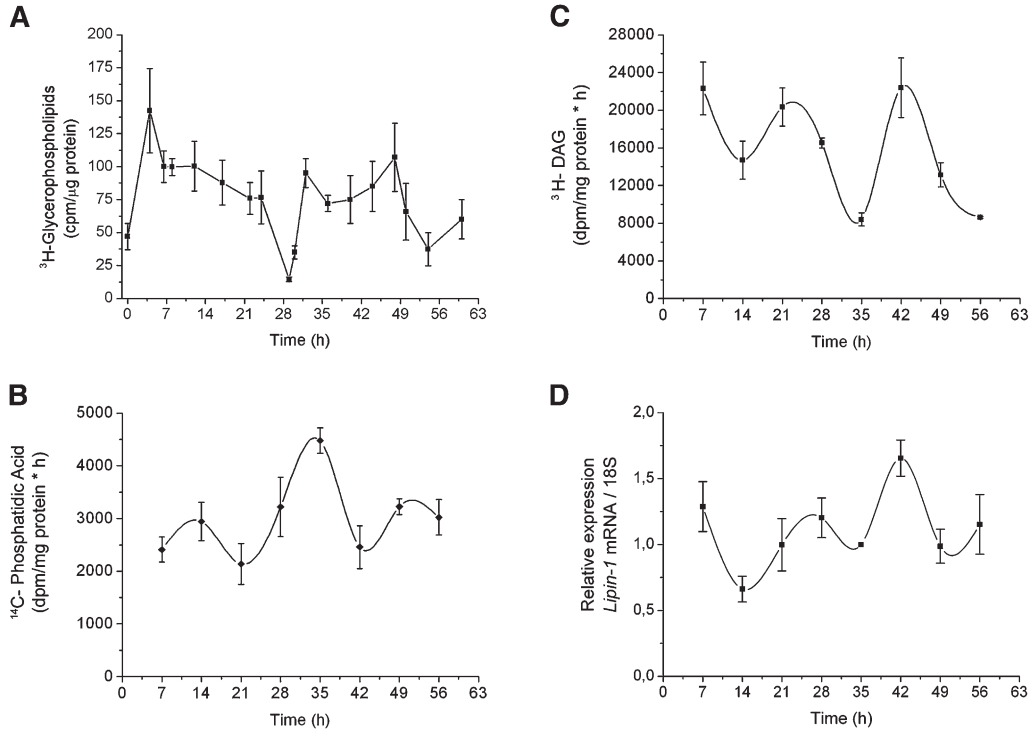

Fig. 1. Daily variation in the labeling of [^{3}H]glycerophospholipids (A), in the activities of LPAAT (B) and PAP-1 (C), and in the expression of *Lipin-1* mRNA (D) in NIH 3T3 cells grown to confluence and synchronized with 50% horse serum shock for 2 h. (A) Levels of incorporation of [^{3}H]glycerol into total phospholipids at different times in synchronized fibroblasts. Cells were given a 30 min labeling pulse of [^{3}H]glycerol at different times through the day after synchronization at time 0. ANOVA revealed a significant effect of time on the labeling of [^{3}H]glycerophospholipids ($P < 0.0004$) with highest levels around 4.5 h and minimum levels at 32 h after stimulation. Data are mean ± SEM (n = 4–10/group) from two independent experiments. (B) LPAAT activity was determined in homogenates of synchronized NIH 3T3 and harvested at different times. The activity was measured by the incorporation of [^{14}C]oleate into LPA. LPAAT activity exhibited significant temporal changes, with the highest activity at 35 h after synchronization and the lowest levels at 21 and 42 h after synchronization ($P < 0.06$ by Kruskal-Wallis ANOVA). (C) PAP-1 activity was determined in NIH 3T3. Kruskal-Wallis ANOVA analysis revealed a significant effect of time on enzyme activity ($P < 0.006$). Mann-Whitney test determined minimum values at 35 and 56 h after synchronization ($P < 0.05$). Results are the mean ± SEM of three independent synchronization experiments (n = 3 technical replicates/group). (D) RT-qPCR was performed on RNA extracted from synchronized NIH 3T3 cells and collected at different times. Although Kruskal-Wallis ANOVA revealed no significant time effect on the levels of *Lipin-1* transcripts, the Mann-Whitney test revealed that minimum values at 14 and 49 h were significantly different from those at 7 and 42 h after synchronization ($P < 0.05$). The results are mean ± SEM of four independent experiments (n = 2 technical replicates/group).

3T3 fibroblasts collected every 7 h at different times ranging from 7 to 56 h (Fig. 1B, C).

De novo synthesis: LPAAT activity. PA, the main precursor of GPLs, is synthesized by the acylation of lysophosphatidic acid (LPA) catalyzed by LPAAT (see Scheme 1). In synchronized cells, the acylation of LPA exhibited a significant temporal variation, with the highest levels of PA production at 35 h after serum stimulation. The lowest levels of PA production by acylation were found at 7–21 h and 42–56 h (Fig. 1B and **Table 5** and **6**). The statistical analysis revealed a significant effect of time on LPAAT activity ($P < 0.06$ by Kruskal-Wallis ANOVA).

De novo synthesis: PAP-1 activity. As precursor of all GPLs, PA is dephosphorylated to DAG by PAPs to synthesize PC and PE (see Scheme 1) (22). Although the activities of two PAP isozymes, PAP-1 and PAP-2, have been found in NIH 3T3 homogenates (data not shown), we focused on PAP-1 activity since it is primarily involved in lipid synthesis in the endoplasmic reticulum. In synchronized cells, PAP-1 activity of NIH 3T3 preparations exhibited a significant temporal variation, with the highest levels of DAG production at 7–21 and 42 h after serum stimulation and the lowest levels at 35 and 56 h (Fig. 1C and Tables 5 and 6). The statistical analysis showed time to have a major effect ($P < 0.006$ by Kruskal-Wallis ANOVA). Pairwise comparisons revealed that levels of activity at 7–21 and 42 h were significantly higher than those at 35 and 56 h. PAP-1 activity is due to the newly defined family of lipin proteins. Herein, we assessed mRNA levels for *lipin-1*, one of the most abundant lipin isoforms, by using primers that recognize three alternatively spliced transcripts of *lipin-1*. The results shown in Fig. 1D exhibit a similar temporal

TABLE 3. One-way ANOVA analysis of incorporation of radiolabeled precursors into GPLs and PCs in quiescent NIH 3T3 fibroblasts

Phospholipid	*P*	Amplitude (%)	Maximum Value/Time (h)	Minimum Value/Time (h)
^{3}H-Glycerophospholipids	0.0004	81	712,500 ± 160,000 (4)	72,000 ± 8,500 (29)
^{3}H-Phosphatidylcholine	0.00001	38	201,000 ± 25,000 (4)	77,000 ± 4,000 (29)
^{32}P-Phosphatidylcholine	0.0001	57	6,600,000 ± 400,000 (5)	1,620,000 ± 280,000 (29)

Statistical analysis was performed with results from three independent experiments (n = 4–6/group) using a one-way Kruskal-Wallis ANOVA to test a time effect. Amplitude (%) was calculated as the $\Delta x/x_{av}$ ratio, in which Δx is the difference between the media of results at all times examined (x_{av}) and the lowest values of phospholipid labeling and the media of results (x_{av}). Maximum and minimum values for each precursor (dpm/mg protein*h) with their corresponding phases of occurrence shown in parentheses are also included to denote the amplitude of each variation along 56 h examined. See text for further detail.

profile to that found for PAP-1 activity. Although the ANOVA did not show a significant effect of time across the 56 h examined, the pairwise comparisons revealed that mRNA levels at 7 and 42 h were significantly higher than those at 14 and 49 h.

Temporal contribution of the LPLAT activity to GPL remodeling

To investigate whether the remodeling of GPLs varies across time, we assessed the activity of LPLATs involved in the reacylation of lysophospholipids (Lands cycle) in synchronized NIH 3T3 cells. We found a remarkable temporal variation in the activity of LPLAT for the different GPLs examined (**Fig. 2** and Tables 5 and 6). The statistical analysis revealed a significant main effect of time for LPLAT activity irrespective of the lysophospholipid examined ($P < 0.02$ by ANOVA) as well as a rhythmic pattern as shown by a linear-circular correlation analysis (Table 6). Posthoc comparisons demonstrated that the maximum lysophosphatidylethanolamine acyltransferase (LPEAT) and lysophosphatidylinositol acyltransferase (LPIAT) activity levels along 21–35 h differ from the minimum values at 14 and 42–49 h after synchronization, whereas the level of lysophosphatidylserine acyltransferase (LPSAT) activity at 28 and 56 h was higher than that from 14 to 21 and from 42 to 49 h (Fig. 2A). We found a significant 2- to 3-fold variation in LPSAT, LPEAT, and LPIAT (Fig. 2) activities between maximal and minimal values. Even though we detected markedly distinct profiles for each lysophospholipid, the highest activity was observed during a temporal window centered at 28 h after stimulation and the lowest around 14 and 42–49 h. Remarkably, the activity peak for all LPLAT measured is in antiphase to the rhythm observed in the metabolic labeling of GPLs, which display minimum levels around 28–32 and 56 h after stimulation (Fig. 1A).

Circadian changes in the labeling of PC in synchronized NIH 3T3 fibroblasts

When we specifically investigated the biosynthesis of PC, the most abundant GPL in eukaryotic cells, a significant temporal variation was observed in the incorporation of [^{32}P]phosphate or [^{3}H]glycerol into PC along a 60 h range (**Fig. 3** and Tables 3 and 4). After the serum shock, levels of [^{3}H]PC increased during the first hour and decreased around 29–32 h. The level of labeling increased again at 36–48 h during the second cycle and significantly decreased at 54–60 h (Fig. 3B). The ANOVA for [^{3}H]PC labeling revealed a significant effect of time ($P < 0.00001$). Labeling of PC with [^{32}P]orthophosphate (indicating both de novo biosynthesis and partial turnover) also displayed a temporal variation: levels were elevated up to 26 h and then decreased significantly at 29–30 h after synchronization. Levels peaked again around 40–50 h and declined significantly at 58 h (Fig. 3A) ($P < 0.0001$ by ANOVA). Moreover, the temporal labeling for both [^{32}P] and [^{3}H] PC exhibited an oscillatory pattern with a period of ~28 h (Tables 3 and 4). These observations are in good agreement with previous findings for the labeling of total [^{32}P] phospholipids (4).

Temporal control of the first step in de novo synthesis of PC catalyzed by the enzyme ChoK

We investigated whether the daily changes observed in the biosynthesis of PC (Fig. 3) were associated with comparable changes in the activity and/or expression of ChoK, the first enzyme in de novo biosynthesis of PC. To this end, we first studied the activity of ChoK in NIH 3T3 cells synchronized by a 2 h serum shock and harvested at different times during 56 h. We found a significant fluctuation across time in the in vitro production of [^{14}C]phosphocholine (Kruskal-Wallis ANOVA, $P < 0.006$) (**Fig. 4A** and Tables 5 and 6). The results showed an oscillating pattern

TABLE 4. Periodic analysis by linear-circular correlation of incorporation of radiolabeled precursors into GPLs and PCs in quiescent NIH 3T3 fibroblasts

Phospholipid	r^2	*P*	Period (τ, h)
^{3}H-Glycerophospholipids	0.4	0.02	28
^{3}H-Phosphatidylcholine	0.6	0.003	28
^{32}P-Phosphatidylcholine	0.5	0.002	28

Statistical analysis was performed with results from three independent experiments (n = 4–6/group) using a periodic analysis by linear-circular correlation with the Spearman coefficient followed by an aleatorization test. Periodic analysis includes r^2 and period (τ) with significance at $P < 0.05$. See text for further detail.

TABLE 5. One-way Kruskal-Wallis ANOVA analysis of enzyme activity and mRNA expression in quiescent NIH 3T3 fibroblasts

	P	Amplitude (%)	Time at Maximum Value (h)	Time at Minimum Value (h)
Enzymatic activity				
PAP-1	0.006	47	21 and 42	35 and 56
ChoK	0.006	13	14–21 and 49–56	7, 35, 42
CCT	0.001	41	6,5 and 35	7–33
LPAAT	0.06	28	35	7–21
LPCAT	0.02	25	21–35 and 56	14 and 42–49
LPEAT	0.01	26	21–35 and 56	14 and 49–56
LPIAT	0.004	18	21–35	7–14 and 42–56
LPSAT	0.004	23	28 and 56	14 and 42
mRNA expression				
ChoKα	0.03	43	14–21	**7** and 28
ChoKβ	NS	—	—	—
CCTα1	NS[a]	—	3	6–36
CCTβ2	0.03	41	9–12	3 and 15–36
PEMT	NS[a]	—	0–7	14–56

Statistical analysis was performed with results from 3–4 independent experiments (n = 3/group) using Kruskal-Wallis one-way analysis to test the time effect. Amplitude (%) was calculated as the $\Delta x/x_{av}$ ratio in which Δx is the difference between the media of results at all times examined considered as 100% (x_{av}) and the lowest values of mRNA expression and the media of results at all times examined (x_{av}). The times at which maximum and minimum values were found for each precursor are included to denote the periodicity of each variation along the 56 h examined. NS, not significant.

[a] Values for *CCTα1* and *PEMT* mRNAs at times of peak differed from other times examined by the Mann-Whitney test. See text for further detail.

of ChoK activity, with higher levels between 14–21 and 49–56 h alternating with lower activity at 7 and 35–42 h. To find out whether the observed rhythmic activity of ChoK was due to similar changes in gene expression at the mRNA level, we studied the temporal profile of *ChoKα* and *ChoKβ* transcripts by RT-qPCR during 56 h (**Fig. 5** and Table 6). The Kruskal-Wallis ANOVA revealed a significant time effect for *ChoKα* mRNA ($P < 0.03$) but not for *ChoKβ* transcript levels. Moreover, the periodic analysis shown in Table 6 indicated that levels of *ChoKα* mRNA oscillates with a period (τ) ~28 h ($P \leq 0.03$) (Fig. 5A and Table 6). Nevertheless, we were unable to detect levels of ChoKα protein by Western blot in the homogenates, likely due to its low expression in nontumor-derived cells (36, 57).

Temporal control of the second step in de novo synthesis of PC catalyzed by CCT

We examined whether the daily changes observed in the biosynthesis of PC involved comparable changes in the activity and/or expression of the key enzyme CCT.

Temporal profiles of the in vitro CCT activity. To this end, we first assessed total CCT enzyme activity in vitro by measuring the formation of [^{14}C]CDP-choline in homogenates of synchronized cells collected at different times from 0 to 36 h. The results showed a significant increase in CCT activity at 6.5 h, followed by a rapid decrease to basal values between 8 and 34 h (Fig. 4B and Tables 5 and 6). The activity picked up again to maximum levels at 35 h after synchronization (Fig. 4B). The Kruskal-Wallis ANOVA

TABLE 6. Periodic analysis by linear-circular correlation of enzyme activity and mRNA expression in quiescent NIH 3T3 fibroblasts

	r^2	*P*	Period (τ, h)
Enzymatic activity			
PAP -1	0.2	NS	28
ChoK	0.5	0.0001	28
CCT	0.008	NS	28
LPAAT	0.07	NS	28
LPCAT	0.12	NS	28
	2.87	0.0001	14
LPEAT	0.4	0.008	28
LPIAT	0.04	NS	28
	0.34	0.01	35
LPSAT	0.900	0.0001	28
mRNA expression			
ChoKα	0.34	0.04	28
ChoKβ	0.016	NS	28
CCTα1	0.005	NS	28
CCTβ2	0.09	NS	28
PEMT	0.005	NS	28

Periodic analysis includes r^2 and period (τ) of 14, 28, or 35 h with significance at $P < 0.05$. See text for further detail. NS, not significant.

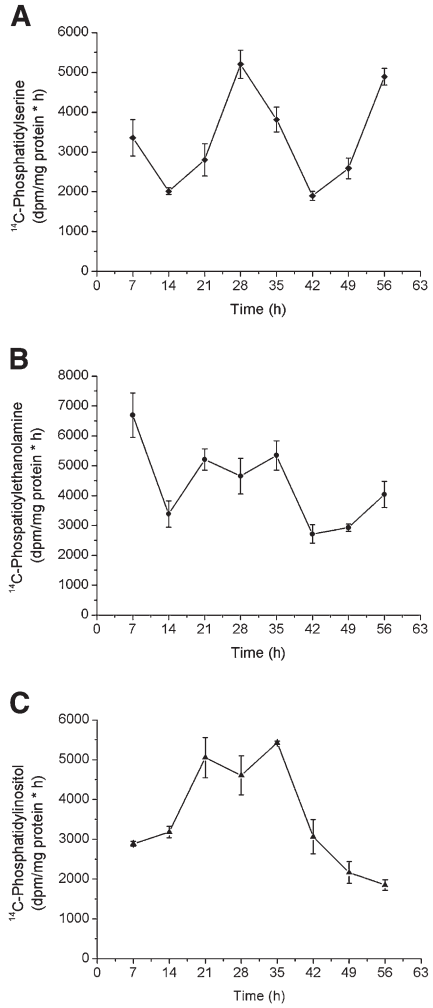

Fig. 2. Daily variation in the different LPLAT activity in NIH 3T3 cells. LPLAT activity was determined in homogenates of NIH 3T3 synchronized by 2 h 50% horse serum shock and harvested at different times. The activity was measured by the incorporation of [^{14}C]oleate into (A) LPS, (B) LPE, and (C) LPI. The LPLAT activity for LPS exhibited temporal changes, with higher activity at 28 and 56 h after synchronization ($P < 0.05$) as determined by Mann-Whitney test. The LPLAT activity for LPE (B) and LPI (C) showed similar temporal patterns, exhibiting higher activity between 21 and 35 h after synchronization ($P < 0.01$ and $P < 0.004$, respectively, by Kruskal-Wallis ANOVA). Results are the mean ± SEM of three independent experiments (n = 3 technical replicates/group).

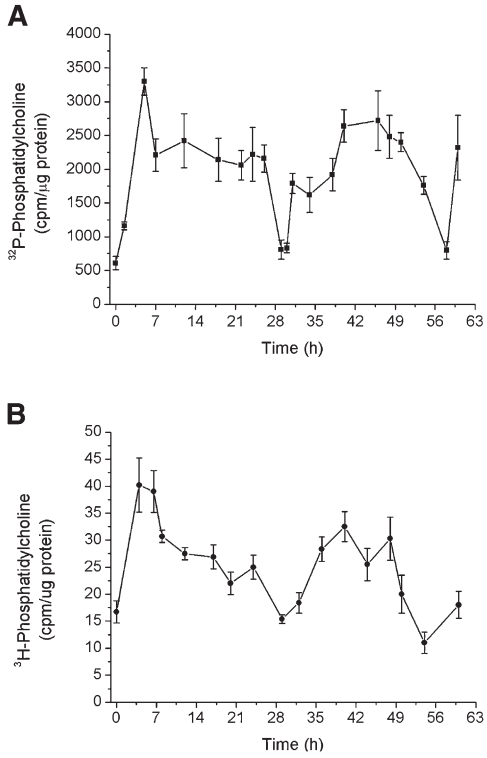

Fig. 3. Daily variation in the labeling of [^{32}P]phosphatidylcholine (A) and of [^{3}H]phosphatidylcholine (B) in NIH 3T3 fibroblasts grown to confluence and synchronized with 50% horse serum shock for 2 h. (A) Labeling of [^{32}P]phosphatidylcholine with [^{32}P]orthophosphate at different times after serum treatment at time 0. Cells were given a 30 min labeling pulse of [^{32}P]orthophosphate at different times after synchronization at time 0. A daily variation was observed with maximum levels at 5 h after treatment and lowest levels at 29 and 58 h ($P < 0.001$ by ANOVA). The results are mean ± SEM of three independent experiments (n = 4–11/group). (B) Levels of incorporation of [^{3}H]glycerol into phosphatidylcholine at different times after serum synchronization. A daily variation was observed with maximum levels at 6.5 h after treatment and lowest levels at 32 h ($P < 0.01$ by ANOVA). Data are mean ± SEM (n = 4–10/group) from two independent experiments.

revealed a significant effect of time on the enzyme activity of synchronized NIH 3T3 cell cultures ($P < 0.001$), with a 2-fold increase in CCT activity at 6.5 and 35 h compared with the activity at all other times examined.

Temporal profiles of CCTα1 and CCTβ2 mRNA expression. The daily variation found in CCT activity in the synchronized cultures of NIH 3T3 fibroblasts could be the result of equivalent changes in levels of mRNA and protein for the different CCT isoforms. We first examined the presence of the different *CCT* isoform mRNAs by RT-PCR. Detectable PCR products were observed for *CCTα1*, *CCTα2*, *CCTβ2*, and *CCTβ3* transcripts compared with positive controls (brain and testis tissues; data not shown). To quantify the most abundant *CCT* transcripts in cell cultures at different times, we assessed the expression of *CCTα1* and *CCTβ2* mRNAs by RT-qPCR (3). Supplementary Fig. II shows the relative levels of *CCTα1* and *CCTβ2* transcripts along 36 h of culture, with highest levels at 3 and 9–12 h after serum shock, respectively. The Kruskal-Wallis ANOVA revealed a significant effect of time for *CCTβ2* mRNA expression ($P < 0.03$) but not for *CCTα1* (Table 6). Nevertheless, *CCTα1* mRNA exhibited an elevated expression at 3 h after synchronization and then returned to basal levels. In contrast, we detected significantly higher levels of *CCTβ2* mRNA at 9–12 h after synchronization and minimum expression at 18–36 h. However, the effect of time observed did not represent a significant oscillation as observed by the linear-circular correlation analysis (Table 6).

Temporal profiles of CCTα and CCTβ protein expression and subcellular localization. We used Western blot analysis and ICC (supplementary Fig. III) to investigate the expression and subcellular localization of the CCTα and CCTβ proteins

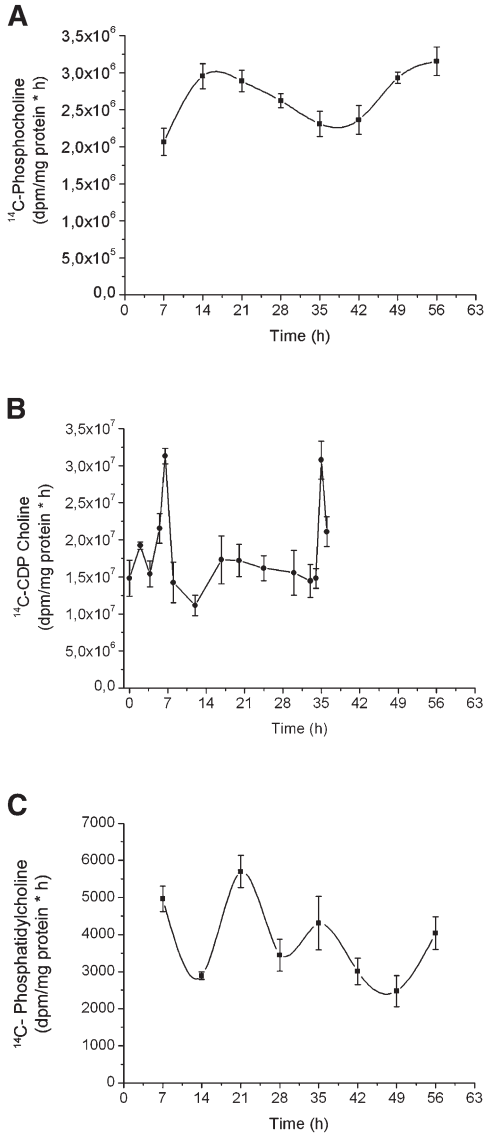

Fig. 4. Daily variation in the PC-synthesizing enzyme activities in NIH 3T3 cells grown to confluence and synchronized with 50% horse serum shock for 2 h. (A) Daily pattern of in vitro ChoK activity in NIH 3T3 cells synchronized by a 2 h serum shock harvested at different times during 56 h. We found ChoK activity in vitro to be time-dependent ($P < 0.006$ by Kruskal-Wallis ANOVA). The results show an oscillating pattern of ChoK activity, with higher levels between 14 and 21 h and 49 and 56 h alternating with lower activity at 7 and 35–42 h. The results are mean ± SEM (triplicate samples from four independent experiments). (B) Daily variation in total CCT activity in NIH 3T3 fibroblasts grown to confluence and synchronized with 50% horse serum shock for 2 h. CCT activity was measured in vitro with total homogenates of cells harvested at different times after serum shock between 0 and 36 h. Results are mean ± SEM of nine independent experiments (n = 3–16/group). The daily variation was observed in total CCT activity ($P < 0.001$ by ANOVA), with highest levels at 6.5 and 35 h after serum shock. (C) LPCAT activity was determined in homogenates of NIH 3T3 synchronized by 2 h 50% horse serum shock and harvested at different times. The activity was measured by the incorporation of [^{14}C] oleate into LPC. The LPCAT activity exhibited a significant temporal variation ($P < 0.02$ by Kruskal-Wallis ANOVA) with the lowest levels around 14 and 49 h after serum shock.

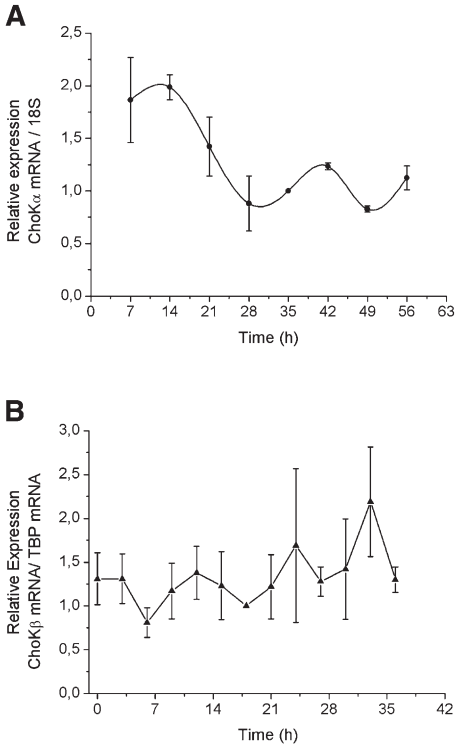

Fig. 5. Temporal expression of *ChoKα* and *ChoKβ* mRNA. RT-qPCR was performed on RNA extracted from NIH 3T3 cells synchronized by a 2 h serum shock and collected at different times. (A) Kruskal-Wallis ANOVA revealed a significant time effect on the levels of *ChoKα* transcripts. Periodic analysis tested by lineal-circular correlation indicated that the levels of ChoKa mRNA oscillated during the time ($P < 0.0001$). (B) *ChoKβ* transcript presented constant levels at all times examined by KW-ANOVA. The results are mean ± SEM (triplicate samples from three independent experiments).

in NIH 3T3 cells at different times after a 2 h serum shock. The Western blot for the CCTβ protein revealed two bands between 49 and 37 kDa, which may correspond to the isoforms CCTβ2 (43 kDa) and CCTβ3 (39 kDa), respectively. These two bands displayed different temporal patterns of expression: band "a" (CCTβ2) presented a peak at 9 h that differs from those at 12–36 h ($P < 0.05$ by Mann-Whitney test), whereas band "b" (CCTβ3) substantially increased by 9–18 h after serum shock ($P < 0.05$ by Mann-Whitney test). In contrast, although the ANOVA revealed no significant effect of time for CCTα, Mann-Whitney test indicated that levels at 3 h differ from those at other times after synchronization ($P < 0.05$). The relative contribution of the different CCT isoforms clearly changes over time, indicating that although CCTα peaks at 0–3 h, the two CCTβ isoforms may act in combination at particular times after serum treatment. In addition, similar changes were observed in the immunoreactivities associated with CCTα and CCTβ proteins at the different times tested by ICC (supplementary Fig. IIIE). Moreover, we determined that CCTα protein was mainly confined to the cell nucleus, whereas the CCTβ2/3 immunofluorescence remained outside the nucleus (supplementary Fig. IIIE). Furthermore, the differential subcellular localization of the two proteins remained constant at all times examined.

Time-related profiles of other enzymes that contribute to the biosynthesis of PC

An alternative PC biosynthetic pathway taking place mainly in the liver has been described in which the enzyme phosphatidylethanolamine methyl transferase (PEMT) converts PE into PC (31). To address whether this pathway contributes to the temporal control of PC metabolism, we evaluated *pemt* mRNA expression by RT-qPCR. We found that levels of *pemt* mRNA displayed a rapid and transient increase in response to the serum shock; however, it did not exhibit a significant circadian rhythmicity (supplementary Fig. IIC and Tables 5 and 6).

In addition, the Lands cycle may also participate in maintaining PC content across time. To this end, we investigated the temporal contribution of LPCAT activity in the production of PC in synchronized NIH 3T3 cells. We found a significant temporal variation in the incorporation of [^{14}C]oleate into PC ($P < 0.02$ by Kruskal-Wallis ANOVA; Tables 5 and 6 and Fig. 4C). Posthoc comparisons demonstrated that the maximum LPCAT activity at 7, 21, and 56 h significantly differ from those at 42–49 h. Moreover, the linear-circular correlation analysis showed that the activity exhibited a daily rhythmicity with a period (τ) of $\sim$14 h (Table 6).

DISCUSSION

In the present work, we described for the first time concerted and sequential changes in specific enzyme activities and/or mRNA expression for the temporal control of GPL metabolism and particularly of PC biosynthesis in synchronized fibroblasts. Nevertheless, not all the steps involved in lipid synthesis and tested here are subject to temporal regulation (see Scheme 1). However, those steps that were shown to be regulated by internal clocks may reflect different levels of transcriptional and posttranscriptional control involving changes in mRNA and protein expression and/or activities for the different synthesizing enzymes investigated.

Immortalized cell lines constitute intriguing models of peripheral oscillators for the study of metabolic oscillations

The results presented here constitute the first report demonstrating the temporal organization of the GPL metabolism in cell-autonomous oscillators regardless of the cell cycle and influence of the central master clock. Cultures of immortalized fibroblasts synchronized by a serum shock displayed daily oscillations in the expression of clock genes (supplementary Fig. I) (4), as well as in several enzymatic steps implicated in the de novo biosynthesis and remodeling of GPLs (see Scheme 1).

Self-sustained oscillatory behavior at the level of gene expression and metabolic activities has been observed in immortalized cell lines and primary cell cultures, regardless of central control or systemic influence (2–5, 42, 58). Recent studies clearly linked the molecular clock with the regulation of lipid metabolism, and the disruption of circadian clocks results in pathophysiological changes resembling the metabolic syndrome, in which lipid metabolism is strongly altered (9, 10, 14, 18, 59).

The cultured fibroblasts used here were quiescent cells grown to confluence and then stimulated with a high concentration of serum that synchronizes endogenous clocks located in individual cells (3, 5) (supplementary Fig. I). Although the 2 h serum shock could trigger cell proliferation, the cell cycle cannot progress in confluent NIH 3T3 cells because they are inhibited by contact (60). Moreover, cultures maintained in a basal serum condition after the serum shock present $\sim$90% of cells arrested at G_0/G_1, a percentage that remained constant at the times examined (0, 2, and 24 h after stimulation; supplementary Fig. I).

Daily variations in phospholipid biosynthesis and gene expression in synchronized NIH 3T3 cell cultures

It has been shown that fibroblasts in culture exhibit circadian rhythms in the biosynthesis of [^{32}P]phospholipids in clear antiphase with the rhythm in *Per1* expression (3, 4). Moreover, after knocking down *Per1* expression, the metabolic rhythm disappeared and cultures of *CLOCK* mutant fibroblasts - cells with an impaired clock mechanism - displayed a loss of rhythmicity in both PER1 expression and phospholipid labeling. These results clearly show a tight control over phospholipid synthesis by the molecular circadian clock in immortalized cell cultures.

In this article, we characterize the oscillatory behavior of GPL de novo biosynthesis and remodeling in cultured fibroblasts after serum synchronization. The metabolic labeling of whole GPLs with [^{3}H]glycerol, and particularly of PC with both ^{3}H-glycerol and [^{32}P]phosphate, reveals significant daily variations with minimum levels at 28–35 and 53–56 h across the 60 h examined (Figs. 1 and 3 and Tables 3 and 4). This finding is fully consistent with our previous report on total [^{32}P]phospholipid labeling (4).

To determine whether the observed changes were a consequence of particular time-regulated enzyme activities, we assessed the activity of the two key biosynthetic enzymes, LPAAT and PAP-1. Several enzymes involved in GPL metabolism have been shown to be highly regulated (42, 43, 48, 61–63). PAP-1 (or lipin), an enzyme that plays an essential role in phospholipid metabolism, dephosphorylates PA to DAG (64, 65). A second type of phosphatidate phosphatase is PAP-2 (or lipid phosphate phosphatase), which is mainly involved in signal transduction mechanisms (66–68). DAG generated by PAP-1 is specifically utilized for PC, PE, and triacylglycerol synthesis, whereas PA is used for PI synthesis through the CDP-DAG pathway (22) (Scheme 1). Although we detected both PAP activities in the cell preparations, we focused our attention on the temporal regulation of PAP-1 activity in relation to its role in GPL biosynthesis. We found that LPAAT and PAP-1 activities exhibit significant daily variations with totally opposite profiles when assessed in synchronized NIH 3T3 preparations collected at different times (Fig. 1B, C). Strikingly, the lowest levels of PAP-1 activity were recorded around 35 and 56 h after synchronization, times at which LPAAT showed the highest activity. Thus, the resulting PA

content could be transiently utilized for other intracellular functions, such as signaling or PI synthesis. In addition, similar temporal patterns with elevated PAP-1 activity and *lipin-1* mRNA levels were found at other times, likely indicating that a higher DAG content can be provided for the de novo synthesis of GPLs during these phases (Fig. 1C, D and Table 5). Strikingly, *lipin-1* has also been reported to oscillate in the liver at the mRNA level by microarray assay (69) and to act as a transcriptional coactivator on a circadian basis (70).

The generation of lysophospholipids is a consequence not only of the prior sterification of glycerol-3-phosphate but also of phospholipase activity as part of the well-known deacylation-reacylation cycle (25). Since LPLAT may reflect the activity of this cycle, we cannot discard the possibility of the differential temporal regulation of PLA or other phospholipases in NIH 3T3 cells. Moreover, the LPLAT activities of the different lysophospholipids examined presented distinct circadian profiles, mostly with highest levels in a time window around 21–35 h, in exact antiphase to [^{3}H]GPL labeling and PAP-1 activity (see Figs. 1A and 2 and Table 5). These observations probably reflect a differential wave of GPLs generated by acylation of LPLAT to keep the membrane homeostasis, likely to give rise to differential phospholipid content and composition in the membrane when de novo lipid synthesis is significantly decreased. This temporal variation may cause significant changes in the fatty acid composition and quality of GPLs, affecting the membrane curvature and fluidity and ultimately regulating the activity and function of different cellular processes (24). Although the reported oscillations are driven by an autonomous clock with a period near 24 h, a few LPLAT activities (LPC and LPIAT, Tables 5 and 6) displayed a different period from 28 h, likely reflecting the fact that the total activity came from different acyltransferases having affinity for the same lysoGPLs, since at least two different LPLAT families with multiple isoenzymes have been described (24).

We are as yet unable to firmly establish whether the changes described in this article are generated by changes in levels of enzyme mRNA and/or protein, by a precise temporal regulation of enzyme activities, by differential accessibility of particular substrates, or by a combination of all these possibilities; and if the latter is the case, whether there is a particular hierarchy in the sequence of such events. Nevertheless, our findings clearly show that the de novo biosynthesis and remodeling of GPLs are subject to endogenous temporal control, likely reflecting *i*) a differential requirement across time of newly synthesized phospholipids for membrane biogenesis and/or generation of second lipid messenger waves, or *ii*) the temporal separation of events within the cell, in addition to the spatial organization of reactions in the different cell compartments. The biogenesis of new membrane is required for a number of cellular processes, including cell division, exocytosis, vesicular traffic, and production of organelles. In fact, we have reported that retinal neurons also display daily rhythms in phospholipid metabolism, which may be necessary for axon and dendrite growth regulation as well as axonal transport (41–43). These metabolic oscillations may represent a general feature of oscillators present either in NIH 3T3 or neuronal cells (41, 42). Moreover, these findings reflect a similar correlation regarding the circadian-regulated synthesis of GPLs and expression of clock genes, such as *Bmal1*, in both cell types.

Time-related mechanisms modulate the biosynthesis of PC in cell cultures

Our observations constitute the first report of significant daily variations in PC biosynthesis in quiescent cultures of NIH 3T3 fibroblasts after synchronization. Indeed, higher levels of precursor incorporation ([^{3}H]glycerol or [^{32}P]phosphate) were found during the first 5–6 h after stimulation along the first cycle and minimum labeling at 28–35 and 53–59 h (Fig. 3). Multiple levels of control may act to regulate the metabolism of PC across time in the cultures. At this point, we can hypothesize that the activation of specific key regulatory synthesizing enzymes at the level of expression and/or activity takes place at particular times after serum shock synchronization.

The variations observed in the biosynthesis of PC in synchronized cultures of fibroblasts (Fig. 3) may be due at least in part to *1*) a higher availability of DAG differentially generated by PAP-1 at certain times (Fig. 1C) and *2*) concerted changes in the activity of the regulatory enzymes ChoK and CCT (Fig. 4A, B). In fact, both ChoK activity and expression for the *ChoKα* isoform mRNA exhibited a significant daily variation in the synchronized NIH 3T3 fibroblasts (Figs. 4A and 5A and Tables 5 and 6). The lowest levels for *ChoKα* were recorded at 28 h after serum stimulation, and the enzyme activity displayed a delayed profile across time, likely reflecting the time required for translation. Strikingly, ChoK has been shown to be strongly expressed in tumor cells (36), and although this enzyme is not the rate-limiting enzyme in PC synthesis, it has been proposed to function as a key regulatory enzyme (27, 32, 33) that seems to be tightly regulated in a circadian manner. Our results suggest that this enzyme may temporally control the biosynthesis of PC in synchronized cells. In addition, the temporal variation in [^{3}H]PC biosynthesis of cell cultures (Fig. 3) is preceded by brief changes in the total activity of CCT (Fig. 4B), the rate-limiting enzyme in the Kennedy pathway, indicating that there are other levels of regulation controlling PC content in the cell. Our findings show two sharp peaks of enzyme activity across a 36 h window, appearing at 6.5 and 35 h after serum stimulation with a 28.5 h separation, resembling the period previously described (4, 5). In this respect, a diurnal variation in CCT activity was reported in the rat retina (71), and changes in CCT activity were associated with those observed in PC synthesis (72–74) along the cell cycle in cultures of different cell lines. The CCT levels and subcellular distribution of both CCT isoforms did not display circadian rhythmicity (supplementary Fig. III), showing nuclear confinement for the CCTα isoform and cytoplasmic localization for CCTβ. Thus, we may infer that the variation in CCT activity indicates enzyme activation by posttranslational modifications

and binding to the endoplasmic reticulum or nuclear membranes (72–75).

An alternative PC biosynthetic pathway has been described in the liver involving PEMT to catalyze the formation of PC from PE (31). Although the contribution of PEMT activity to the synthesis of PC in NIH 3T3 cells and whether it is regulated by the endogenous clock is still unknown, we only found a rapid and transient increase in PEMT mRNA levels in response to the serum shock but no detectable circadian oscillation (supplementary Fig. IIC).

In addition to clock regulation, PC metabolism may be regulated by homeostatic mechanisms, such as substrate availability, the state of enzyme activities (posttranslational modifications and subcellular localization), and rate-limiting steps, among others (22). In this respect, cellular levels of CTP, a substrate for CCT, can control PC synthesis as well as choline and phosphocholine availability and the cellular concentration of DAG (27, 32).

Overall, our observations lead us to infer that the biosynthesis of whole GPLs and particularly of PC in NIH 3T3 fibroblast cultures undergoes clear temporal variations somehow sensing the time of day in relation to external cues (food, temperature, hormones, etc.). The circadian regulation of GPL synthesis may be important for a better understanding of the temporal organization of a number of cellular processes, such as the membrane renewal, vesicular trafficking, exocytosis, membrane protein activity (receptors, channels, etc.) and/or second messenger reservoir changes.

The authors thank Mrs. Susana Deza and Gabriela Schachner for their technical assistance and Dr. Pilar Crespo for her excellent support and collaboration. The authors are grateful to Drs. S. Jackowski and N. Ridgway for the kind gift of the CCT antibodies.

REFERENCES

1. Dunlap, J. C., J. J. Loros, and P. J. DeCoursey. 2004. Chronobiology: Biological Timekeeping. Sinauer Associates, Sunderland, MA.
2. Mohawk, J. A., C. B. Green, and J. S. Takahashi. 2012. Central and peripheral circadian clocks in mammals. *Annu. Rev. Neurosci.* **35:** 445–462.
3. Balsalobre, A., F. Damiola, and U. Schibler. 1998. A serum shock induces circadian gene expression in mammalian tissue culture cells. *Cell.* **93:** 929–937.
4. Marquez, S., P. Crespo, V. Carlini, E. Garbarino-Pico, R. Baler, B. L. Caputto, and M. E. Guido. 2004. The metabolism of phospholipids oscillates rhythmically in cultures of fibroblasts and is regulated by the clock protein PERIOD 1. *FASEB J.* **18:** 519–521.
5. Nagoshi, E., S. A. Brown, C. Dibner, B. Kornmann, and U. Schibler. 2005. Circadian gene expression in cultured cells. *Methods Enzymol.* **393:** 543–557.
6. Reddy, A. B., N. A. Karp, E. S. Maywood, E. A. Sage, M. Deery, J. S. O'Neill, G. K. Wong, J. Chesham, M. Odell, K. S. Lilley, et al. 2006. Circadian orchestration of the hepatic proteome. *Curr. Biol.* **16:** 1107–1115.
7. Huang, W., K. M. Ramsey, B. Marcheva, and J. Bass. 2011. Circadian rhythms, sleep, and metabolism. *J. Clin. Invest.* **121:** 2133–2141.
8. Sahar, S., and P. Sassone-Corsi. 2012. Regulation of metabolism: the circadian clock dictates the time. *Trends Endocrinol. Metab.* **23:** 1–8.
9. Bass, J., and J. S. Takahashi. 2010. Circadian integration of metabolism and energetics. *Science.* **330:** 1349–1354.
10. Asher, G., and U. Schibler. 2011. Crosstalk between components of circadian and metabolic cycles in mammals. *Cell Metab.* **13:** 125–137.
11. Eckel-Mahan, K. L., V. R. Patel, R. P. Mohney, K. S. Vignola, P. Baldi, and P. Sassone-Corsi. 2012. Coordination of the transcriptome and metabolome by the circadian clock. *Proc. Natl. Acad. Sci. USA.* **109:** 5541–5546.
12. Menger, G. J., G. C. Allen, N. Neuendorff, S. S. Nahm, T. L. Thomas, V. M. Cassone, and D. J. Earnest. 2007. Circadian profiling of the transcriptome in NIH/3T3 fibroblasts: comparison with rhythmic gene expression in SCN2.2 cells and the rat SCN. *Physiol. Genomics.* **29:** 280–289.
13. Hughes, M. E., L. DiTacchio, K. R. Hayes, C. Vollmers, S. Pulivarthy, J. E. Baggs, S. Panda, and J. B. Hogenesch. 2009. Harmonics of circadian gene transcription in mammals. *PLoS Genet.* **5:** e1000442.
14. Bray, M. S., and M. E. Young. 2011. Regulation of fatty acid metabolism by cell autonomous circadian clocks: time to fatten up on information? *J. Biol. Chem.* **286:** 11883–11889.
15. Green, C. B., J. S. Takahashi, and J. Bass. 2008. The meter of metabolism. *Cell.* **134:** 728–742.
16. Sookoian, S., C. Gemma, T. F. Gianotti, A. Burgueno, G. Castano, and C. J. Pirola. 2008. Genetic variants of Clock transcription factor are associated with individual susceptibility to obesity. *Am. J. Clin. Nutr.* **87:** 1606–1615.
17. Takahashi, J. S., H. K. Hong, C. H. Ko, and E. L. McDearmon. 2008. The genetics of mammalian circadian order and disorder: implications for physiology and disease. *Nat. Rev. Genet.* **9:** 764–775.
18. Maury, E., K. M. Ramsey, and J. Bass. 2010. Circadian rhythms and metabolic syndrome: from experimental genetics to human disease. *Circ. Res.* **106:** 447–462.
19. Durgan, D. J., and M. E. Young. 2010. The cardiomyocyte circadian clock: emerging roles in health and disease. *Circ. Res.* **106:** 647–658.
20. Froy, O. 2010. Metabolism and circadian rhythms - implications for obesity. *Endocr. Rev.* **31:** 1–24.
21. van Meer, G., D. R. Voelker, and G. W. Feigenson. 2008. Membrane lipids: where they are and how they behave. *Nat. Rev. Mol. Cell Biol.* **9:** 112–124.
22. Hermansson, M., K. Hokynar, and P. Somerharju. 2011. Mechanisms of glycerophospholipid homeostasis in mammalian cells. *Prog. Lipid Res.* **50:** 240–257.
23. Kennedy, E. P., and S. B. Weiss. 1956. The function of cytidine coenzymes in the biosynthesis of phospholipides. *J. Biol. Chem.* **222:** 193–214.
24. Shindou, H., and T. Shimizu. 2009. Acyl-CoA:lysophospholipid acyltransferases. *J. Biol. Chem.* **284:** 1–5.
25. Shindou, H., D. Hishikawa, T. Harayama, K. Yuki, and T. Shimizu. 2009. Recent progress on acyl CoA: lysophospholipid acyltransferase research. *J. Lipid Res.* **50(Suppl.):** S46–S51.
26. Exton, J. H. 1994. Phosphatidylcholine breakdown and signal transduction. *Biochim. Biophys. Acta.* **1212:** 26–42.
27. Kent, C. 2005. Regulatory enzymes of phosphatidylcholine biosynthesis: a personal perspective. *Biochim. Biophys. Acta.* **1733:** 53–66.
28. Gehrig, K., R. B. Cornell, and N. D. Ridgway. 2008. Expansion of the nucleoplasmic reticulum requires the coordinated activity of lamins and CTP:phosphocholine cytidylyltransferase alpha. *Mol. Biol. Cell.* **19:** 237–247.
29. Cui, Z., and M. Houweling. 2002. Phosphatidylcholine and cell death. *Biochim. Biophys. Acta.* **1585:** 87–96.
30. Vance, D. E., and J. E. Vance. 2009. Physiological consequences of disruption of mammalian phospholipid biosynthetic genes. *J. Lipid Res.* **50(Suppl.):** S132–S137.
31. Li, Z., and D. E. Vance. 2008. Phosphatidylcholine and choline homeostasis. *J. Lipid Res.* **49:** 1187–1194.
32. Araki, W., and R. J. Wurtman. 1998. How is membrane phospholipid biosynthesis controlled in neural tissues? *J. Neurosci. Res.* **51:** 667–674.
33. Marcucci, H., L. Paoletti, S. Jackowski, and C. Banchio. 2010. Phosphatidylcholine biosynthesis during neuronal differentiation and its role in cell fate determination. *J. Biol. Chem.* **285:** 25382–25393.
34. Aoyama, C., H. Liao, and K. Ishidate. 2004. Structure and function of choline kinase isoforms in mammalian cells. *Prog. Lipid Res.* **43:** 266–281.

35. Wu, G., and D. E. Vance. 2010. Choline kinase and its function. *Biochem. Cell Biol.* **88:** 559–564.
36. Gallego-Ortega, D., T. Gomez del Pulgar, F. Valdes-Mora, A. Cebrian, and J. C. Lacal. 2011. Involvement of human choline kinase alpha and beta in carcinogenesis: a different role in lipid metabolism and biological functions. *Adv. Enzyme Regul.* **51:** 183–194.
37. Glunde, K., Z. M. Bhujwalla, and S. M. Ronen. 2011. Choline metabolism in malignant transformation. *Nat. Rev. Cancer.* **11:** 835–848.
38. Karim, M., P. Jackson, and S. Jackowski. 2003. Gene structure, expression and identification of a new CTP:phosphocholine cytidylyltransferase beta isoform. *Biochim. Biophys. Acta.* **1633:** 1–12.
39. Jackowski, S. 1994. Coordination of membrane phospholipid synthesis with the cell cycle. *J. Biol. Chem.* **269:** 3858–3867.
40. Diaz-Munoz, M., J. Suarez, R. Hernandez-Munoz, and V. Chagoya de Sanchez. 1987. Day-night cycle of lipidic composition in rat cerebral cortex. *Neurochem. Res.* **12:** 315–321.
41. Guido, M. E., E. Garbarino Pico, and B. L. Caputto. 2001. Circadian regulation of phospholipid metabolism in retinal photoreceptors and ganglion cells. *J. Neurochem.* **76:** 835–845.
42. Garbarino-Pico, E., A. R. Carpentieri, P. I. Castagnet, S. J. Pasquare, N. M. Giusto, B. L. Caputto, and M. E. Guido. 2004. Synthesis of retinal ganglion cell phospholipids is under control of an endogenous circadian clock: daily variations in phospholipid-synthesizing enzyme activities. *J. Neurosci. Res.* **76:** 642–652.
43. Garbarino-Pico, E., D. J. Valdez, M. A. Contin, S. J. Pasquare, P. I. Castagnet, N. M. Giusto, B. L. Caputto, and M. E. Guido. 2005. Rhythms of glycerophospholipid synthesis in retinal inner nuclear layer cells. *Neurochem. Int.* **47:** 260–270.
44. Gehrig, K., T. A. Lagace, and N. D. Ridgway. 2009. Oxysterol activation of phosphatidylcholine synthesis involves CTP:phosphocholine cytidylyltransferase alpha translocation to the nuclear envelope. *Biochem. J.* **418:** 209–217.
45. Bradford, M. M. 1976. A rapid and sensitive method for the quantitation of microgram quantities of protein utilizing the principle of protein-dye binding. *Anal. Biochem.* **72:** 248–254.
46. Guido, M. E., and B. L. Caputto. 1990. Labeling of retina and optic tectum phospholipids in chickens exposed to light or dark. *J. Neurochem.* **55:** 1855–1860.
47. Weiss, S. J., J. S. McKinney, and J. W. Putney, Jr. 1982. Regulation of phosphatidate synthesis by secretagogues in parotid acinar cells. *Biochem. J.* **204:** 587–592.
48. Castagnet, P. I., and N. M. Giusto. 2002. Effect of light and protein phosphorylation on photoreceptor rod outer segment acyltransferase activity. *Arch. Biochem. Biophys.* **403:** 83–91.
49. Folch, J., M. Lees, and G. H. Sloane Stanley. 1957. A simple method for the isolation and purification of total lipides from animal tissues. *J. Biol. Chem.* **226:** 497–509.
50. Pasquare de Garcia, S. J., and N. M. Giusto. 1986. Phosphatidate phosphatase activity in isolated rod outer segment from bovine retina. *Biochim. Biophys. Acta.* **875:** 195–202.
51. Pasquare, S. J., and N. M. Giusto. 1993. Differential properties of phosphatidate phosphohydrolase and diacylglyceride lipase activities in retinal subcellular fractions and rod outer segments. *Comp. Biochem. Physiol. B.* **104:** 141–148.
52. Giusto, N. M., and N. G. Bazan. 1979. Phospholipids and acylglycerols biosynthesis and 14CO2 production from [14C]glycerol in the bovine retina: the effects of incubation time, oxygen and glucose. *Exp. Eye Res.* **29:** 155–168.
53. Weinhold, P. A., L. Charles, M. E. Rounsifer, and D. A. Feldman. 1991. Control of phosphatidylcholine synthesis in Hep G2 cells. Effect of fatty acids on the activity and immunoreactive content of choline phosphate cytidylyltransferase. *J. Biol. Chem.* **266:** 6093–6100.
54. Vance, D. E., S. D. Pelech, and P. C. Choy. 1981. CTP: phosphocholine cytidylyltransferase from rat liver. *Methods Enzymol.* **71(Pt. C):** 576–581.
55. Nieto, P. S., V. A. Acosta-Rodriguez, D. J. Valdez, and M. E. Guido. 2010. Differential responses of the mammalian retinal ganglion cell line RGC-5 to physiological stimuli and trophic factors. *Neurochem. Int.* **57:** 216–226.
56. Mardia, K. V. 1976. Linear-circular correlation coefficients and rhythmometry. *Biometrika.* **63:** 403–405.
57. Ramirez de Molina, A., A. Rodriguez-Gonzalez, R. Gutierrez, L. Martinez-Pineiro, J. Sanchez, F. Bonilla, R. Rosell, and J. Lacal. 2002. Overexpression of choline kinase is a frequent feature in human tumor-derived cell lines and in lung, prostate, and colorectal human cancers. *Biochem. Biophys. Res. Commun.* **296:** 580–583.
58. Garbarino-Pico, E., A. R. Carpentieri, M. A. Contin, M. I. Sarmiento, M. A. Brocco, P. Panzetta, R. E. Rosenstein, B. L. Caputto, and M. E. Guido. 2004. Retinal ganglion cells are autonomous circadian oscillators synthesizing N-acetylserotonin during the day. *J. Biol. Chem.* **279:** 51172–51181.
59. Turek, F. W., C. Joshu, A. Kohsaka, E. Lin, G. Ivanova, E. McDearmon, A. Laposky, S. Losee-Olson, A. Easton, D. R. Jensen, et al. 2005. Obesity and metabolic syndrome in circadian Clock mutant mice. *Science.* **308:** 1043–1045.
60. Kuppers, M., C. Ittrich, D. Faust, and C. Dietrich. 2010. The transcriptional programme of contact-inhibition. *J. Cell. Biochem.* **110:** 1234–1243.
61. de Arriba Zerpa, G. A., M. E. Guido, D. F. Bussolino, S. J. Pasquare, P. I. Castagnet, N. M. Giusto, and B. L. Caputto. 1999. Light exposure activates retina ganglion cell lysophosphatidic acid acyl transferase and phosphatidic acid phosphatase by a c-fos-dependent mechanism. *J. Neurochem.* **73:** 1228–1235.
62. Giusto, N. M., S. J. Pasquare, G. A. Salvador, and M. G. Ilincheta de Boschero. 2010. Lipid second messengers and related enzymes in vertebrate rod outer segments. *J. Lipid Res.* **51:** 685–700.
63. Giusto, N. M., G. A. Salvador, P. I. Castagnet, S. J. Pasquare, and M. G. Ilincheta de Boschero. 2002. Age-associated changes in central nervous system glycerolipid composition and metabolism. *Neurochem. Res.* **27:** 1513–1523.
64. Donkor, J., M. Sariahmetoglu, J. Dewald, D. N. Brindley, and K. Reue. 2007. Three mammalian lipins act as phosphatidate phosphatases with distinct tissue expression patterns. *J. Biol. Chem.* **282:** 3450–3457.
65. Reue, K., and D. N. Brindley. 2008. Thematic review series: glycerolipids. Multiple roles for lipins/phosphatidate phosphatase enzymes in lipid metabolism. *J. Lipid Res.* **49:** 2493–2503.
66. Giusto, N. M., S. J. Pasquare, G. A. Salvador, P. I. Castagnet, M. E. Roque, and M. G. Ilincheta de Boschero. 2000. Lipid metabolism in vertebrate retinal rod outer segments. *Prog. Lipid Res.* **39:** 315–391.
67. Brindley, D. N. 2004. Lipid phosphate phosphatases and related proteins: signaling functions in development, cell division, and cancer. *J. Cell. Biochem.* **92:** 900–912.
68. Pasquare, S. J., G. A. Salvador, and N. M. Giusto. 2004. Phospholipase D and phosphatidate phosphohydrolase activities in rat cerebellum during aging. *Lipids.* **39:** 553–560.
69. Panda, S., M. P. Antoch, B. H. Miller, A. I. Su, A. B. Schook, M. Straume, P. G. Schultz, S. A. Kay, J. S. Takahashi, and J. B. Hogenesch. 2002. Coordinated transcription of key pathways in the mouse by the circadian clock. *Cell.* **109:** 307–320.
70. Li, M. D., C. M. Li, and Z. Wang. 2012. The role of circadian clocks in metabolic disease. *Yale J. Biol. Med.* **85:** 387–401.
71. Ikemoto, A., A. Fukuma, Y. Fujii, and H. Okuyama. 2000. Diurnal rhythms of retinal phospholipid synthetic enzymes are retained but their activities are decreased in rats under alpha-linolenic acid deficiency. *Arch. Biochem. Biophys.* **383:** 108–113.
72. Jackowski, S. 1996. Cell cycle regulation of membrane phospholipid metabolism. *J. Biol. Chem.* **271:** 20219–20222.
73. Jackowski, S., and P. Fagone. 2005. CTP: Phosphocholine cytidylyltransferase: paving the way from gene to membrane. *J. Biol. Chem.* **280:** 853–856.
74. Sugimoto, H., C. Banchio, and D. E. Vance. 2008. Transcriptional regulation of phosphatidylcholine biosynthesis. *Prog. Lipid Res.* **47:** 204–220.
75. Elena, C., and C. Banchio. 2010. Specific interaction between E2F1 and Sp1 regulates the expression of murine CTP:phosphocholine cytidylyltransferase alpha during the S phase. *Biochim. Biophys. Acta.* **1801:** 537–546.
76. Garbarino-Pico, E., S. Niu, M. D. Rollag, C. A. Strayer, J. C. Besharse, and C. B. Green. 2007. Immediate early response of the circadian polyA ribonuclease nocturnin to two extracellular stimuli. *RNA.* **13:** 745–755.
77. Nakahata, Y., M. Akashi, D. Trcka, A. Yasuda, and T. Takumi. 2006. The in vitro real-time oscillation monitoring system identifies potential entrainment factors for circadian clocks. *BMC Mol. Biol.* **7:** 5.